Supporting information

Ferroelectricity-enhanced potassium-ion storage in van der Waals layered $CuInP_2S_6$

*Po-Wen Chien,† Yu-Bo Hung,† Yi-Chun Yang and Hsing-Yu Tuan**

*P.-W. Chien, Y.-B. Hung, Y.-C. Yang, H.-Y. Tuan**

Department of Chemical Engineering, National Tsing Hua University, Hsinchu 30013, Taiwan

Email: hytuan@che.nthu.edu.tw

†: These authors contributed equally to this work and share first authorship.

Table S1. Crystallographic parameters of $CuInP_2S_6$ refined by the Rietveld method.

Site	Atom	x	y	z	Occ
Cu_1	Cu	0.0957	0.3355	0.3869	0.875
Cu_2	Cu	-0.069	0.335	0.149	0.1
In_1	In	0	0.00192	0.25	1
P_1	P	0.5686	0.169	0.3491	1
P_2	P	0.4505	0.1674	0.1788	1
S_1	S	0.2808	0.1512	0.395	1
S_2	S	0.2332	0.1645	0.893	1
S_3	S	0.7845	0.0177	0.395	1
S_4	S	0.74	0.1727	0.1336	1
S_5	S	0.7555	0.1747	0.6404	1
S_6	S	0.2722	-0.0057	0.6379	1
a=6.1057		b=10.5569		c=13.5973	
R_{wp}=5.19				R_p=4.29	

Table S2. ICP concentrations of the as-synthesized $CuInP_2S_6$ (CIPS)

Sample	**Cu (at%)**	**In (at%)**	**P (at%)**	**S (at%)**
$CuInP_2S_6$	**11.69**	**11.43**	**20.94**	**55.94**

Table S3. Comparison of diffusion coefficients between CIPS@G and $FePS_3$@G at different stages.

Stage / D_K^+	**Stage I**	**Stage II**	**Stage III**
CIPS@G	1.19×10^{-10}	3.33×10^{-11}	1.12×10^{-11}
$FePS_3$@G	1.61×10^{-11}	1.98×10^{-11}	1.98×10^{-11}

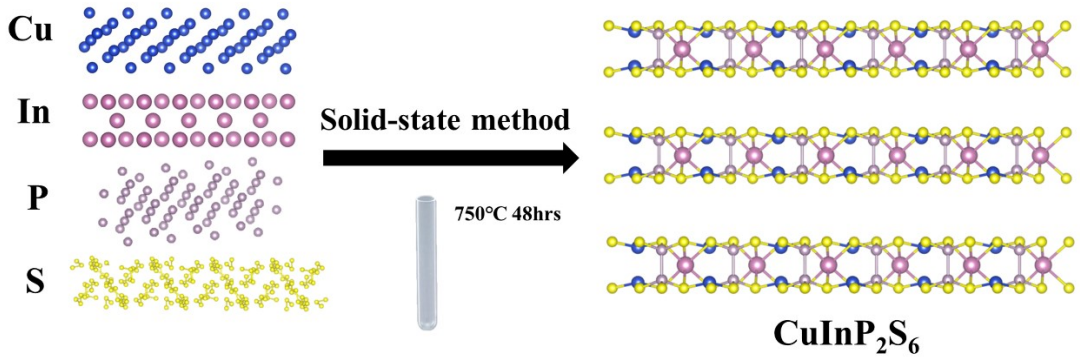

Figure S1. Schematic of the synthesis process of CIPS.

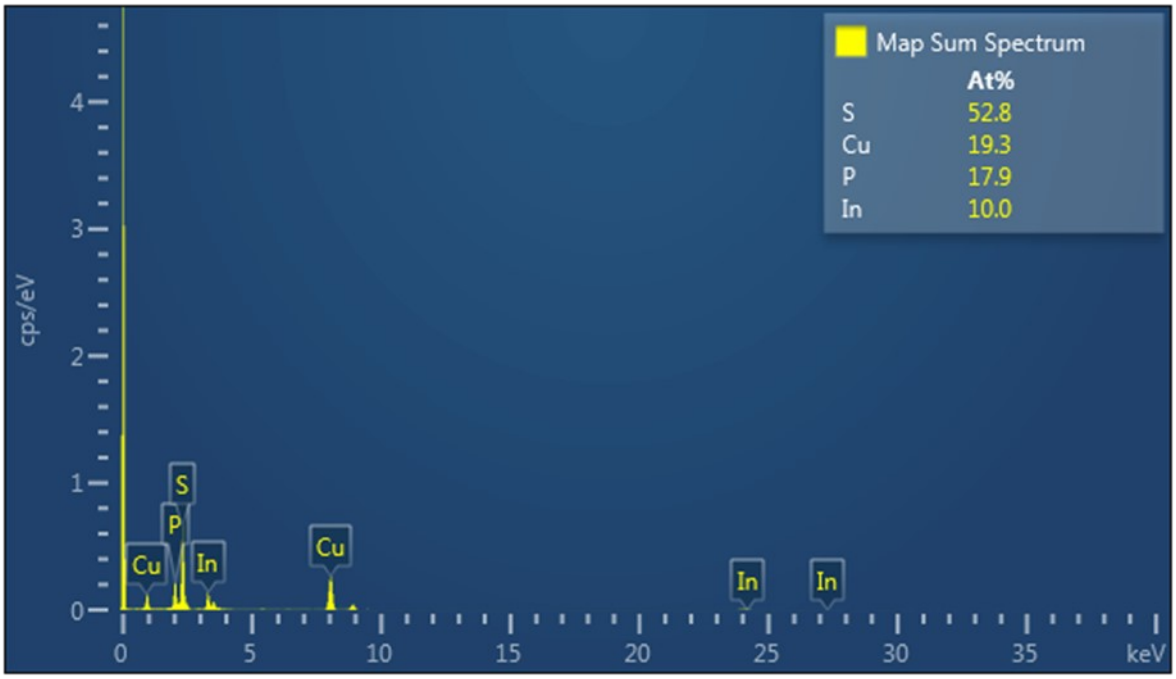

Figure S2. EDS mapping result of CIPS.

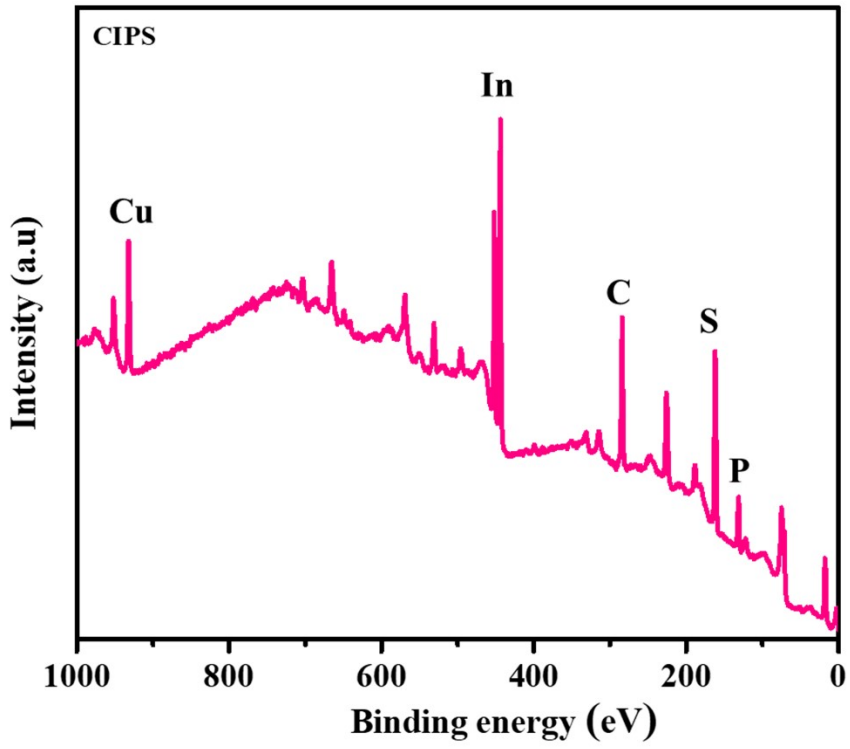

Figure S3. The full survey XPS spectrum of CIPS.

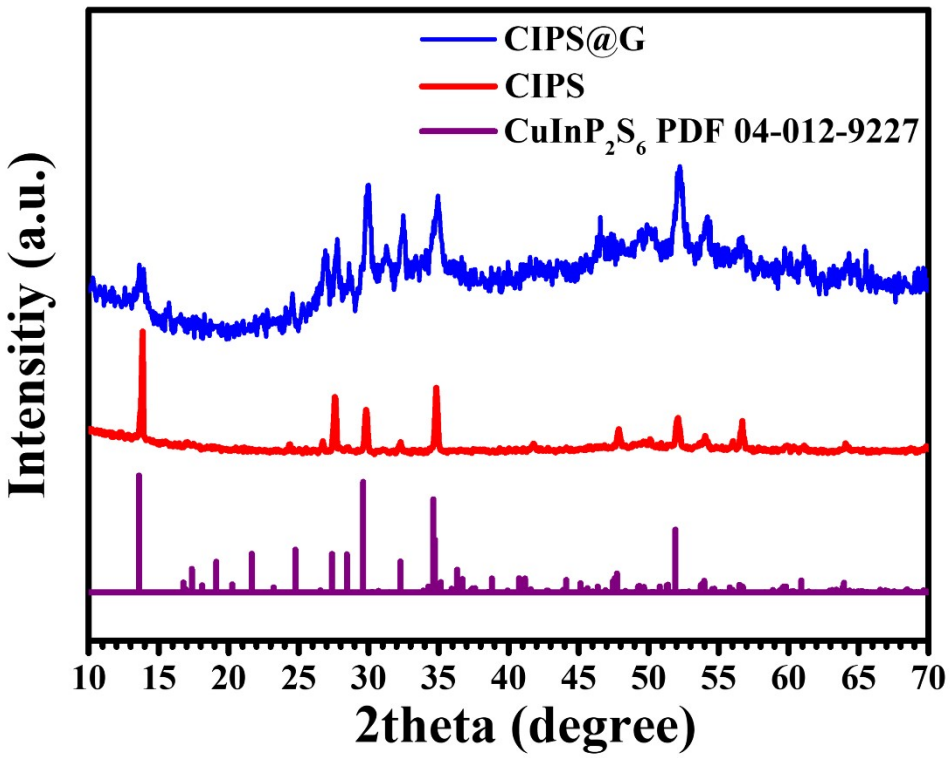

Figure S4. XRD pattern of CIPS@G.

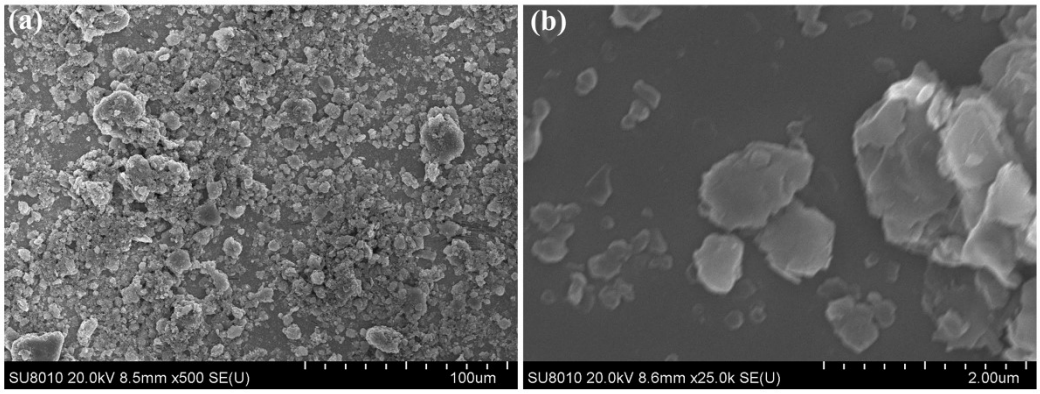

Figure S5. SEM image of CIPS@G.

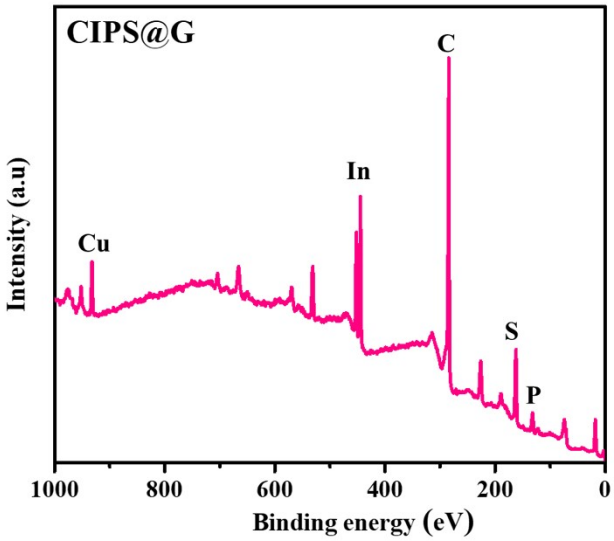

Figure S6. The full survey XPS spectrum of CIPS@G.

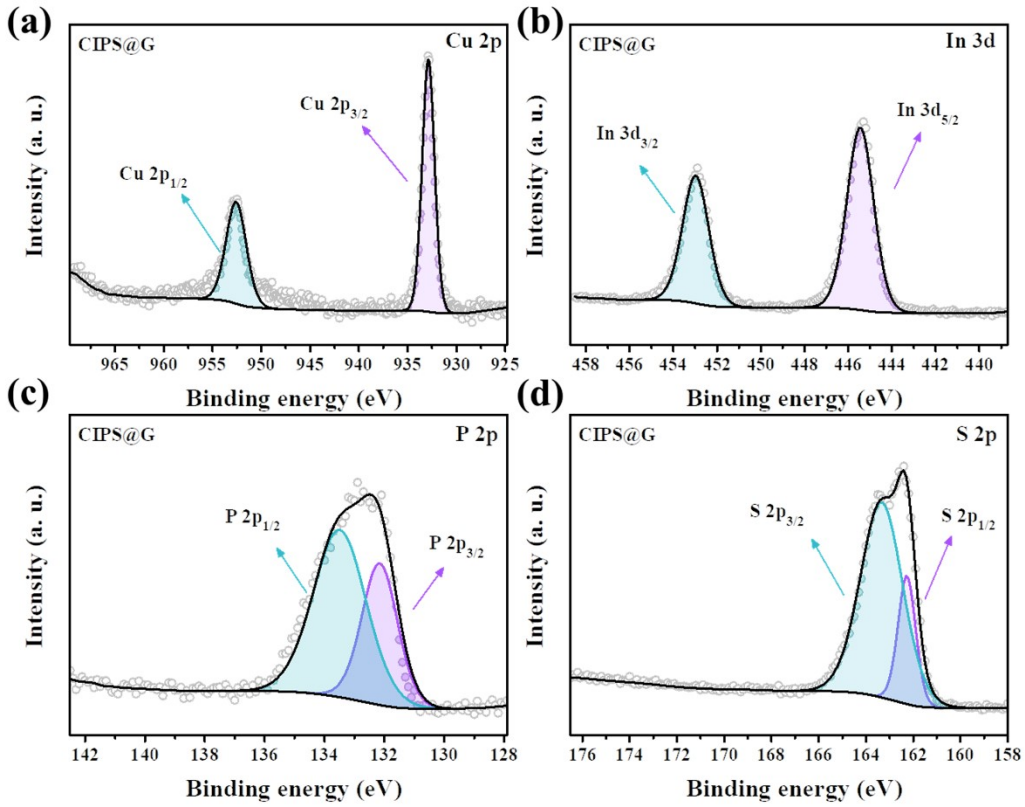

Figure S7. High-resolution (a) Cu 2p, (b) In 3d, (c) P 2p, and (d) S 2p XPS spectra of CIPS@G nanoflakes.

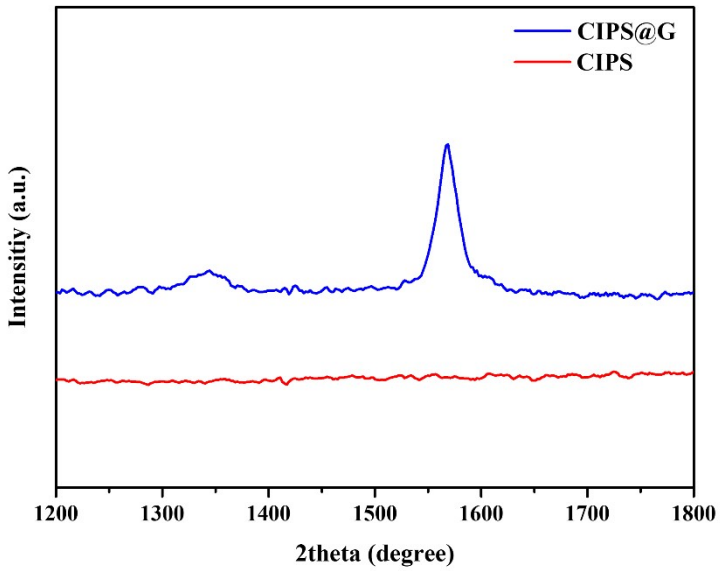

Figure S8. Raman spectra of CIPS and CIPS@G.

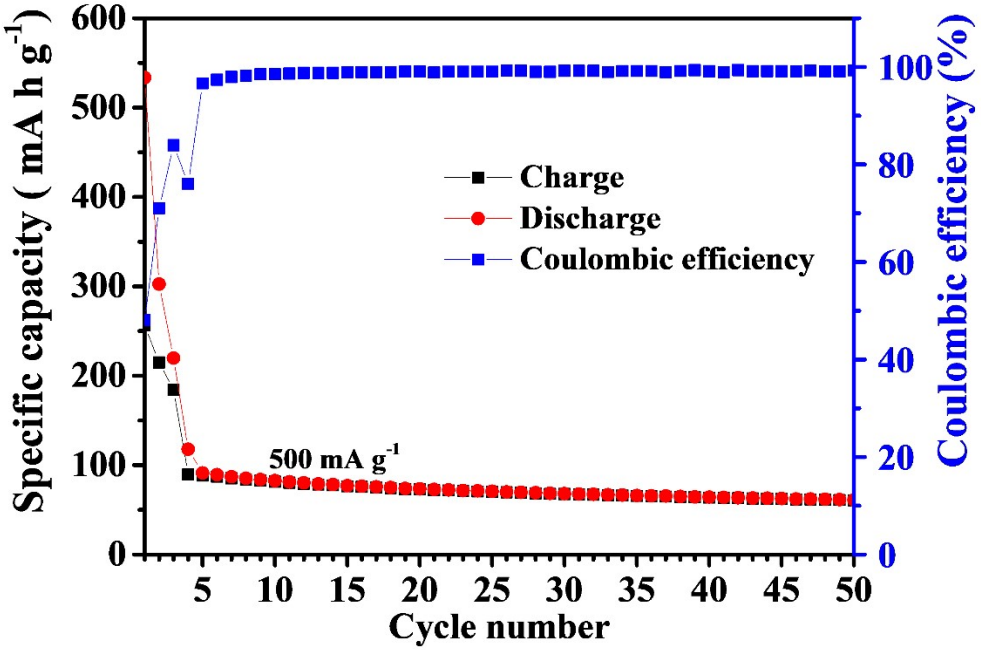

Figure S9. Electrochemical performance of pure CIPS.

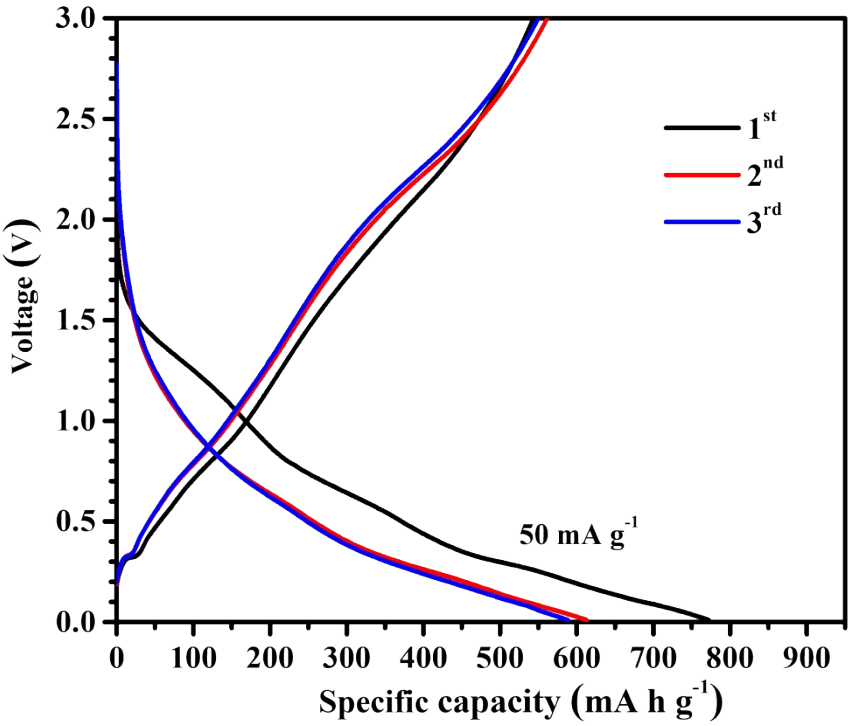

Figure S10. GCD curve of CIPS@G at a current density of 50 mA g^{-1}.

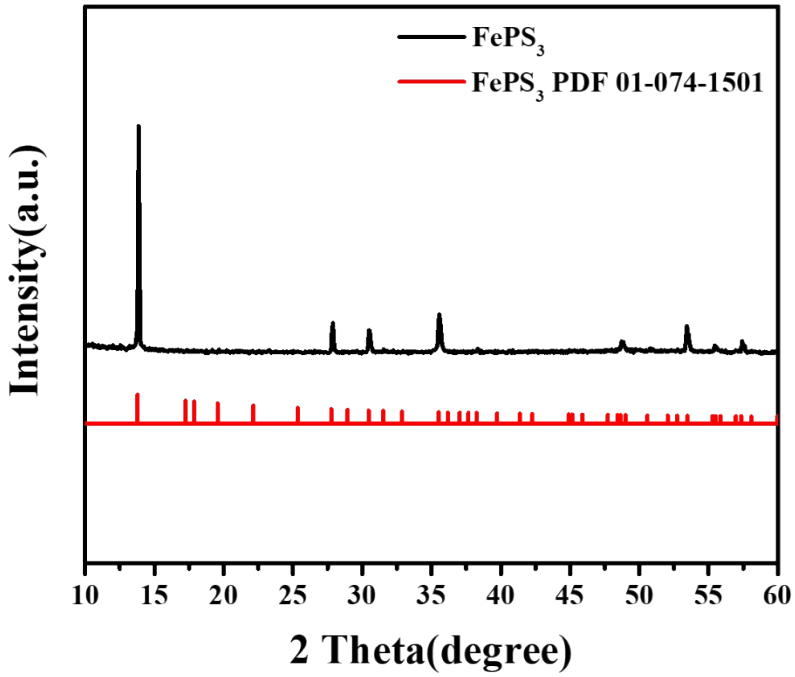

Figure S11. XRD pattern of $FePS_3$.

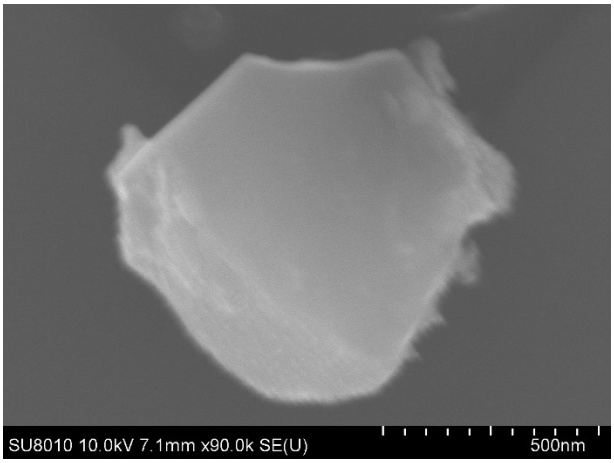

Figure S12. SEM image of $FePS_3$@G.

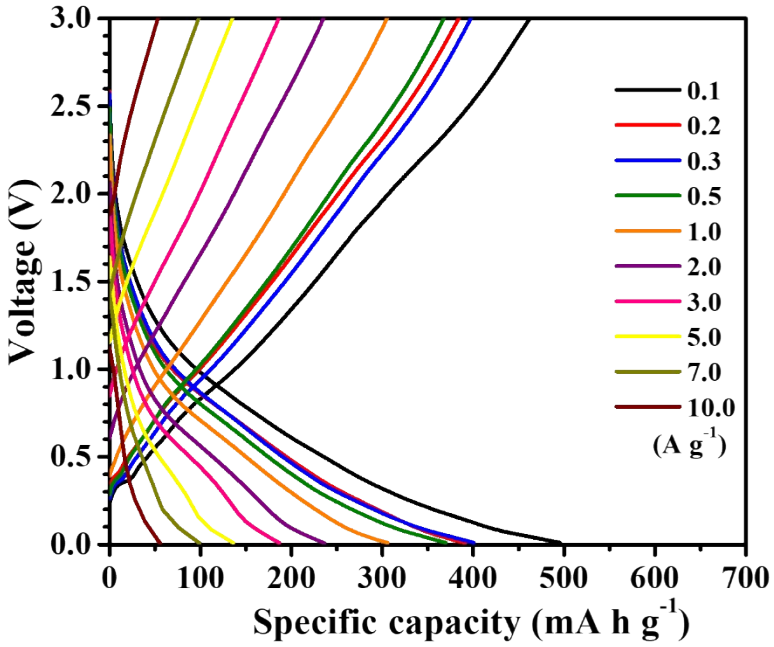

Figure S13. Galvanostatic charge/discharge curves of CIPS@G at various current densities.

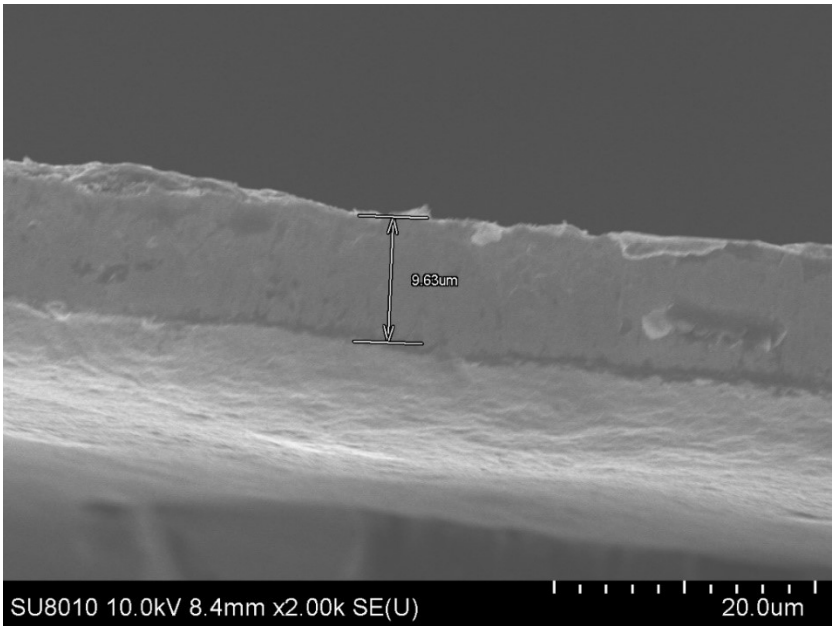

Figure S14. Cross-sectional SEM images and the thickness of CIPS@G electrodes.

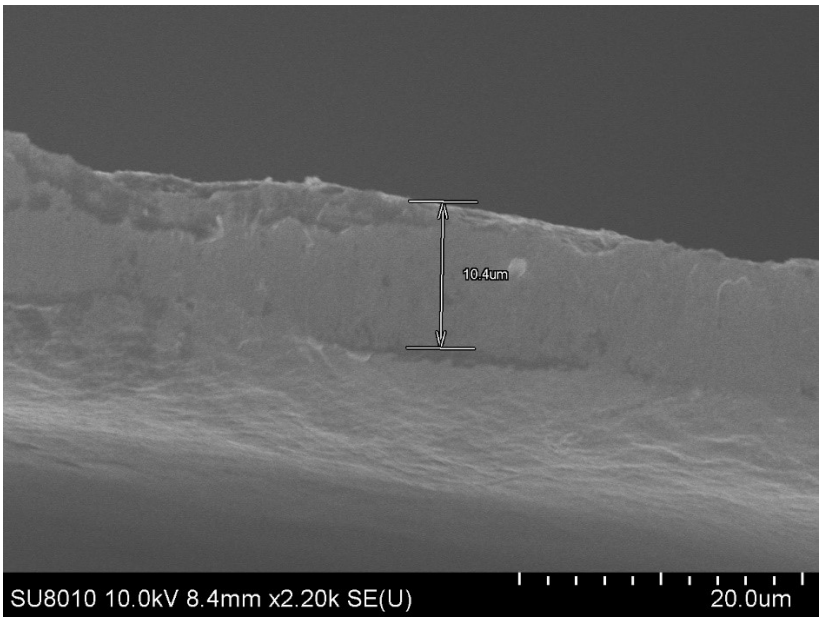

Figure S15. Cross-sectional SEM images and the thickness of $FePS_3$@G electrodes.

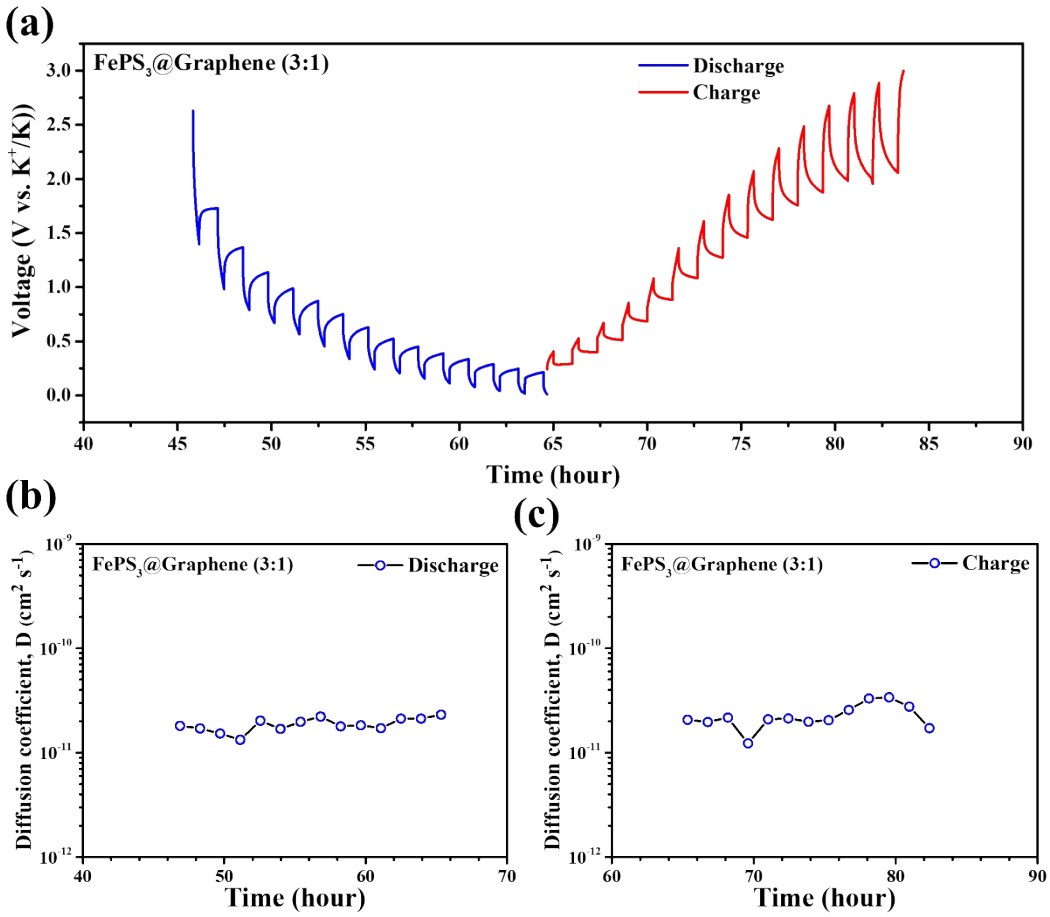

Figure S16. (a) GITT curves of $FePS_3$@G with 20 min current pulse of 50 mA g^{-1} followed by 1 hour relaxation and corresponding diffusion coefficients of (b) discharge and (c) charge process.

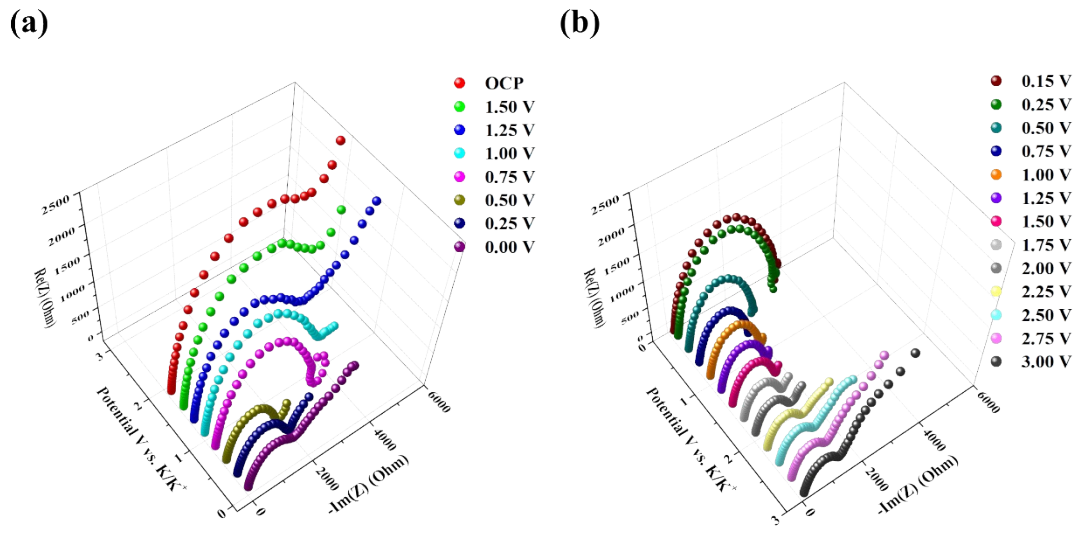

Figure S17. In-situ EIS test performed in selected potentials. (a) Discharging process.(b) Charging process.

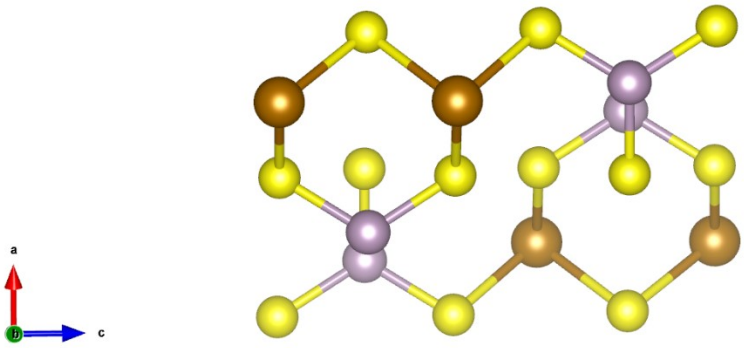

Figure S18. Crystal structure of $FePS_3$.

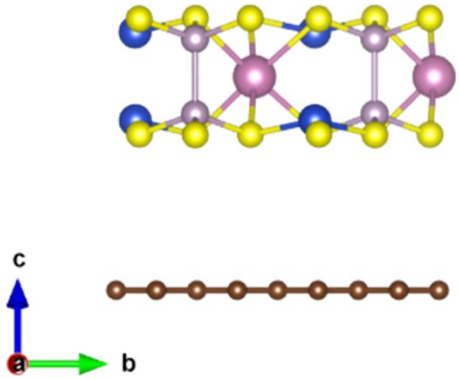

Figure S19. Crystal structure of CIPS@G.

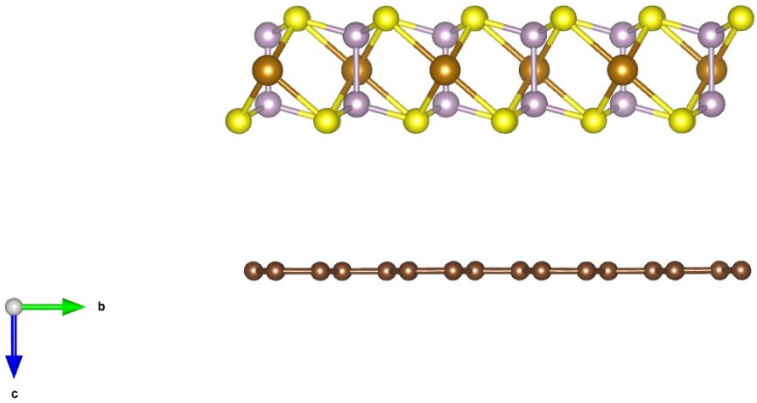

Figure S20. Crystal structure of $FePS_3$@G.

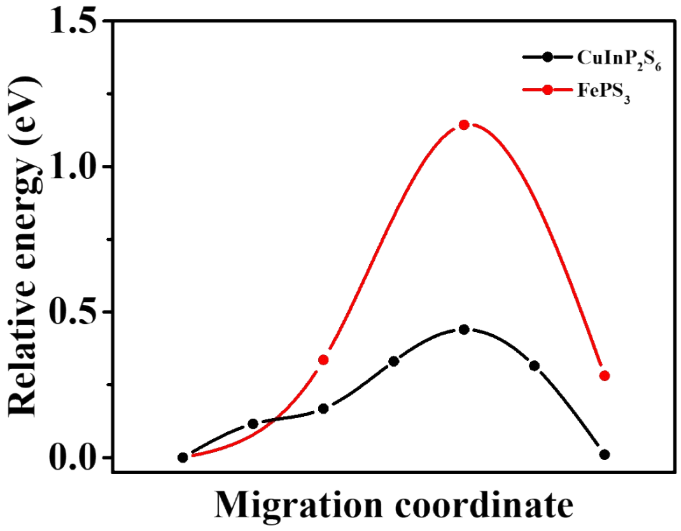

Figure S21. Calculated energy barriers of K between CIPS layers and graphene, and between $FePS_3$ and graphene.

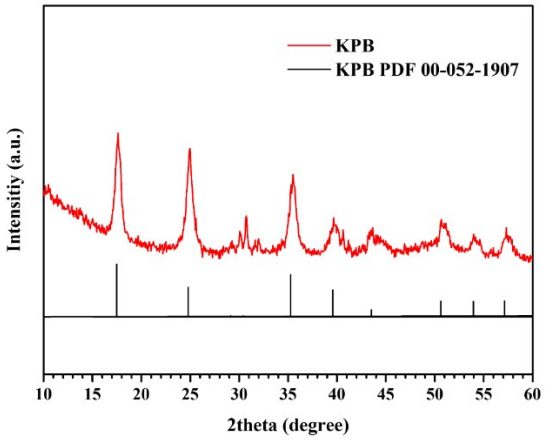

Figure S22. XRD pattern of PB.

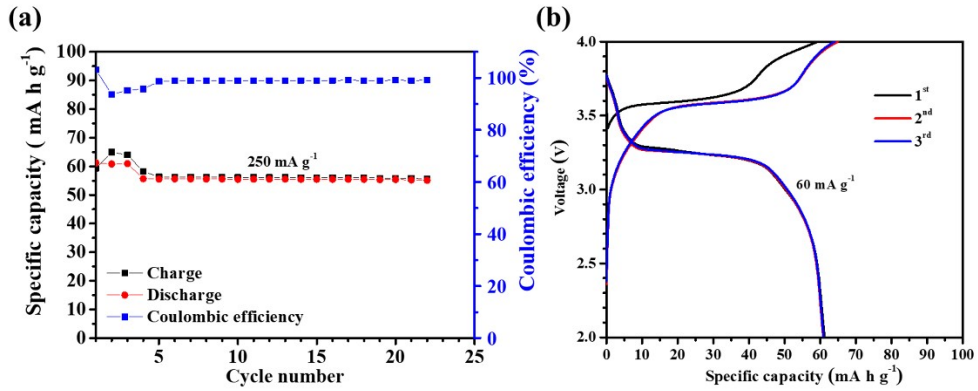

Figure S23. (a) Cycling performances of PB at 250 mA g^{-1} and (b) corresponding galvanostatic charge-discharge curves.

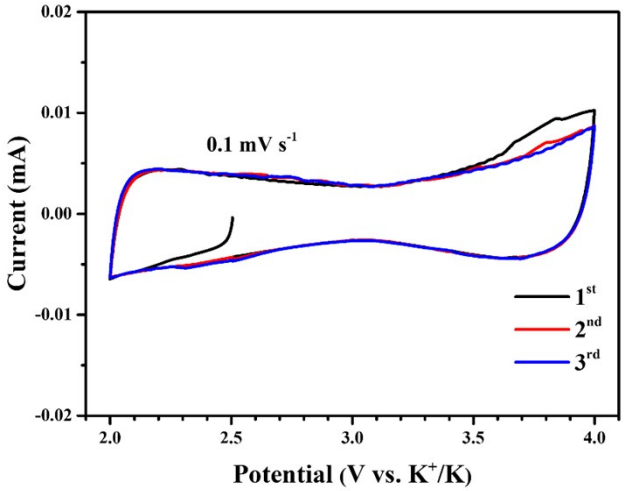

Figure S24. Cyclic voltammetry curves of AC electrodes at 0.1 mV s^{-1}.